

Discretization of Stator Current of Induction Motor Using Predictive Control

Yasin Koçak¹, Nevra Bayhan²

¹Department of Electrical- Electronics Engineering, National Defence University, Institute of Atatürk Strategic Studies and Graduate, İstanbul, Türkiye

²Department of Electrical and Electronics Engineering, İstanbul University-Cerrahpaşa, Faculty of Engineering, İstanbul, Türkiye

Cite this article as: Y. Koçak and N. Bayhan, "Discretization of stator current of induction motor using predictive control," *Electrica*, 24(2), 489-502, 2024.

ABSTRACT

In predictive control of induction motors, control signals are adjusted by predicting the future behavior of the motor. These predictions are made on important parameters such as motor speed, current, and torque, and are supported by real-time data. In general, in model predictive control (MPC) method, the input and output of the system are optimized using cost functions based on reference values. Although the induction motor operates in continuous time, discretization methods are needed for performing the necessary current switching and feedback control with microprocessors. For reference speed tracking in this study, the stator current of a three-phase induction motor with specifications of 60 Hz, 50 HP, and 460 V was decomposed for the first time using Crank–Nicholson, Verlet integration, and Runge–Kutta Ralston methods, which are finite control set (FCS)-MPC discretization methods. In this paper, we compared the Forward Euler, Runge–Kutta 4, Runge–Kutta Ralston, Taylor series, Crank–Nicolson, and Verlet integration techniques, which are FCS-MPC methods, with the conventional discrete-time indirect field oriented control (IFOC) method for speed control of induction motors. Based on the simulation data obtained from the induction motor, overshoot, settling time, reference speed root mean square value, and total harmonic distortion values were taken into account. The Verlet integration method had the least settling time than other methods, in the range of 0–4 s, including nominal speed transitions. When the response signals were examined, it was seen that the Verlet integration method gave the lowest settling time and overshoot percentage values for the 4–8 s, while the Forward Euler method gave the lowest settling time and overshoot percentage values for the 8–10 s.

Index Terms—Discretization, finite set control, induction motor, indirect field oriented control (IFOC), model predictive control (MPC), Verlet integration

I. INTRODUCTION

Induction motors (IMs) are widely used in many industries due to their low cost, robustness, and reliability, and they are essentially multi-phase machines connected to an AC power supply in either the stator or the rotor [1, 2]. The control of IM drives is generally divided into as scalar and vector control. Scalar control only requires magnitude control. However, scalar control has a poor dynamic response and combined torque/speed characteristics. With vector control, the dynamic response of the IM drive has been improved. Vector control is also known as field-oriented control (FOC). Field-oriented control, being an adaptive control method based on the rotor flux model, is a popular technique for low-speed induction motors [3–7]. In literature on induction motor articles, the indirect field-oriented control (IFOC) method previously utilized speed and current controllers for outer-loop and inner-loop controls to manage flux and torque. However, with the active use of proportional-integral (PI) controllers, the need for flux sensors has been eliminated, and sensorless operation provides an advantage in system control [8, 9]. However, the use of linear controllers in the speed control loop reduces the speed control performance with unknown disturbances and mechanical parameter changes. For this reason, recently, model predictive control (MPC) has emerged as an alternative in the control of power converters and electric drives [10, 11]. Due to the structure of the controllers, discrete-time prediction-based control introduces a cumulative cost function and is particularly effective in terms of control strategy when applied to real-time systems compared to classical control methods [12]. Model predictive control, evaluating torque, flux, and current errors in terms of cost function, offers advantages over traditional control methods [13]. The MPC approach uses a mathematical model of the system to predict its behavior within a certain time frame. By combining control objectives, predicted variables, and system constraints, an optimization problem is solved, and as a result, the implementation of control actions is ensured [14, 15]. With respect to the implementation method, MPC used in

Corresponding author:

Nevra BAYHAN

E-mail:

nevra@iuc.edu.tr

Received: March 26, 2024

Revision Requested: April 2, 2024

Last Revision Received: April 3, 2024

Accepted: April 20, 2024

Publication Date: May 17, 2024

DOI: 10.5152/electrica.2024.24042



Content of this journal is licensed under a Creative Commons Attribution-NonCommercial 4.0 International License.

electric drives can be classified as finite control set MPC (FCS-MPC) and continuous control set MPC (CCS-MPC). Finite control set MPC typically utilizes all possible switching states of power converters, and control variables can only be selected from among the possible switching states in each control cycle, hence the control variables are relatively optimal rather than absolute, and the switching frequency of the converter in FCS-MPC is not fixed [16–18]. When comparing the classic control method with the FCS-MPC method in terms of the number of commutations per second, it is necessary to use the FCS-MPC control scheme to reduce the number of commutations [19]. When evaluated in terms of cost function parameters, the FCS-MPC method, which is a control method for induction motors, is primarily examined in two main parts: predictive current control (PCC) and predictive torque control (PTC). The cost function of FCS-MPC-based direct torque control is different from PCC. This is because flux and torque values are used in the cost function [20–22]. In FCS-MPC, a voltage-switching-based cost function is used to select the voltage vector closest to the reference vector by examining all possible states in the cost function, and this method requires a high amount of calculations [23]. Due to its fixed switching frequency, CCS-MPC is typically preferred over FCS-MPC for second-order DC/DC converters such as boost, buck, buck–boost, and non-inverting buck–boost converters [24].

Conventional Forward Euler and Backward Euler methods are employed in the cost function when the discretization accuracy requirements are insufficient, resorting to different transformations. The necessary transformations should be selected to be compatible with predetermined frame models of stator and rotor fluxes, both in the cost function calculation and observer design [25–28]. In conventional MPC, since the weighting factor is constant, some studies design a basic weighting factor, provide transformations in the cost functions, and define the parameters used with different algorithms [29–31]. In some studies for the optimization of the FCS-MPC structure, the prediction model is realized via Taylor series expansion [32]. With this model, the minimization of the cost function can be easily achieved without the need for online optimization [33]. While Euler methods produce a highly oscillatory current reference, the second-order Taylor discretization of the mechanical model ensures smooth reference tracking with only a small overshoot [34]. In addition to the Taylor series method, studies have compared the Euler, Tustin, Runge–Kutta 4, and Runge–Kutta 2 methods in terms of the dynamic response of parameters such as α – β stator current, rotor flux linkage, rotor shaft speed error, reference speed tracking, and similar motor parameters [35, 36]. Model predictive control method is very advantageous in industries where dynamic performance is important, such as industries where induction motors are used. Total harmonic distortion (THD) negatively impacts the overall performance of the system. Some studies have used the predictive current control method to minimize THD, where stator currents are calculated using torque and speed values directly related to motor dynamics, so studies have been conducted for the predictive optimization of conventional FCS-MPC [37–39].

The contributions of this study are summarized as follows:

- In this study, Runge–Kutta Ralston, Verlet integration, and Crank–Nicholson methods have been employed in the FCS-MPC of induction motors in the stator cost function. Reference speed tracking and distortions in stator current are compared based on the methods used.

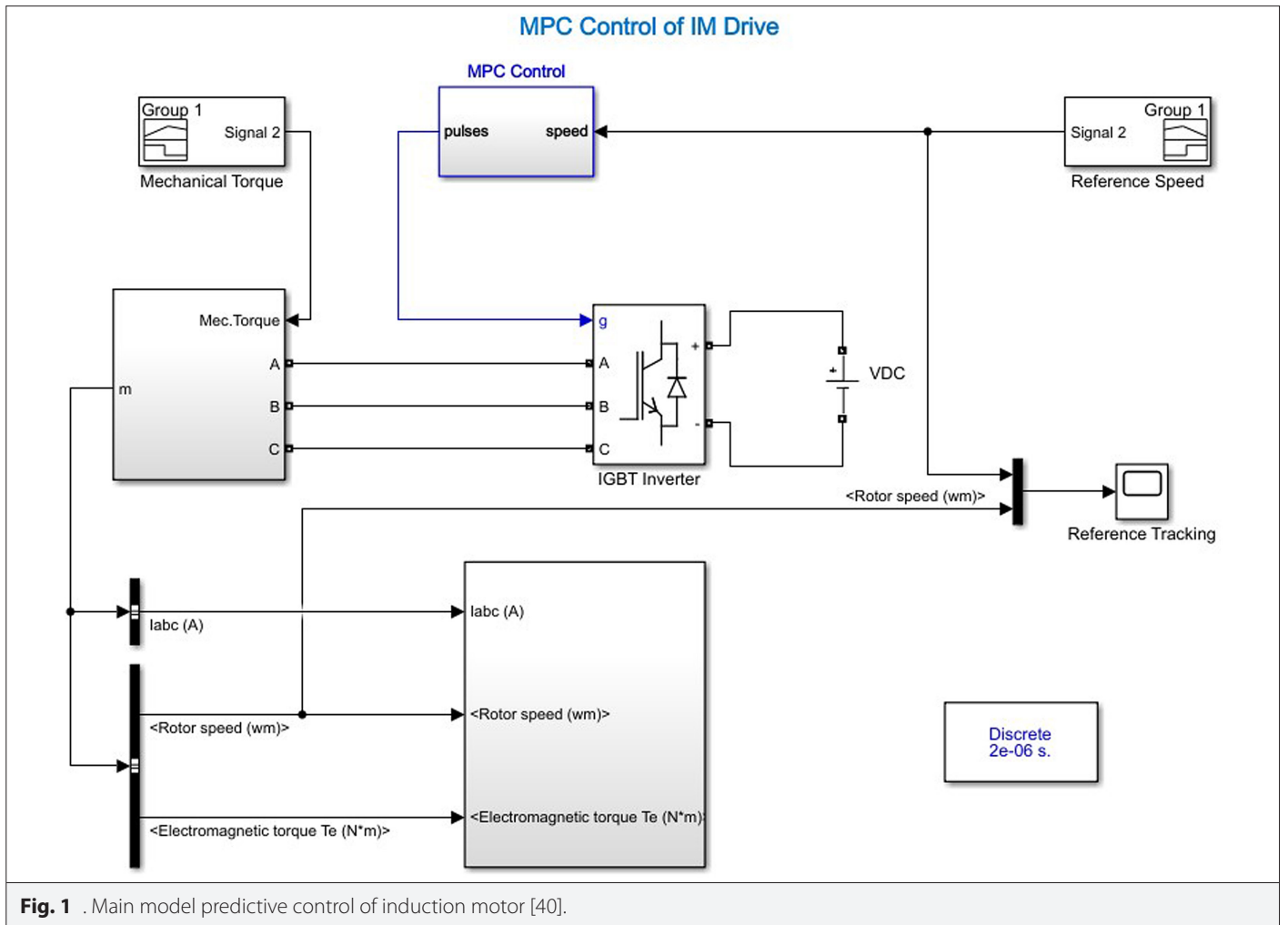
- Predictive control algorithms were used for the drive system to ensure the optimum level of overshoot, settling time, and THD effects when using the induction motor.
- The stator current of the induction motor was examined and compared with the traditional IFOC method and six discretization methods of FCS-MPC (Runge–Kutta Ralston, Verlet integration, Crank–Nicholson, Forward Euler, Fourth Order Runge–Kutta, Taylor series).
- Verlet integration method had the least settling time than other methods, in the range of 0–4 s, including nominal speed transitions. When the response signals were examined, it was seen that the Verlet integration method gave the lowest settling time and overshoot percentage values for the 4–8 s, while the Forward Euler method gave the lowest settling time and overshoot percentage values for the 8–10 s. When examined in terms of settling time values, it was observed that the lowest settling time method was the Verlet integration method in the positive region (186 rad/s reference speed) and negative region (149 rad/s reference speed). It was observed that the Verlet integration method had the second lowest settling time value after the Forward Euler method in the positive region (223 rad/s reference speed).
- It has been observed that the IFOC method has less distortion in average harmonic distortion than the FCS-MPC discretization methods due to its control structure. The method with the highest average harmonic distortion is the FCS-MPC Forward Euler discretization method. Among the FCS-MPC methods, the method with the least average harmonic distortion is the Crank–Nicholson discretization method. The method furthest from the reference speed value of 180.7 rad/s is the Crank–Nicholson discretization method with an root mean square (RMS) value of 170 rad/s.

This paper is structured as follows: the MPC model of the induction motor is described in Section II. Applied discretization methods are explained in Section III. The simulation results are compared in Section IV. Some concluding remarks are included in Section V.

II. CONTROL MODEL OF INDUCTION MOTOR

In this article, the MPC method and indirect FOC method of the induction motor are examined. For the control circuit of the induction motor, a driver and an induction motor are needed. The MPC MATLAB–Simulink model structure of the induction motor control with 60 Hz, 50 HP, and 460 V values is shown in Fig. 1. The reference speed control of the induction motor is achieved by driving the insulated-gate bipolar transistor (IGBT) inverter block depicted in Fig. 1 with a predictive controller. Fig. 1 is derived from [40–41] in terms of its main characteristics and is utilized in this study for the FCS-MPC method. In an industrial-type induction motor, the rated power is high. Its working principle is to provide movement through the induction of a magnetic field. Since there is no mechanical connection between the rotor and the stator, the speed of the rotor in an induction motor is not exactly equal to the rotation speed of the magnetic field of the stator. Therefore, during the operation of the motor, a difference occurs between the rotation speed in the rotor magnetic field and the rotation speed of the stator magnetic field. This difference can lead to wave distortions that cause harmonics to be produced.

The simulation study of the FCS-MPC model is shown in Fig. 2. In Fig. 2, initially, the difference between the reference speed and the speed generated by the motor was taken for calculating the reference stator current required by the MPC. As illustrated in the figure,



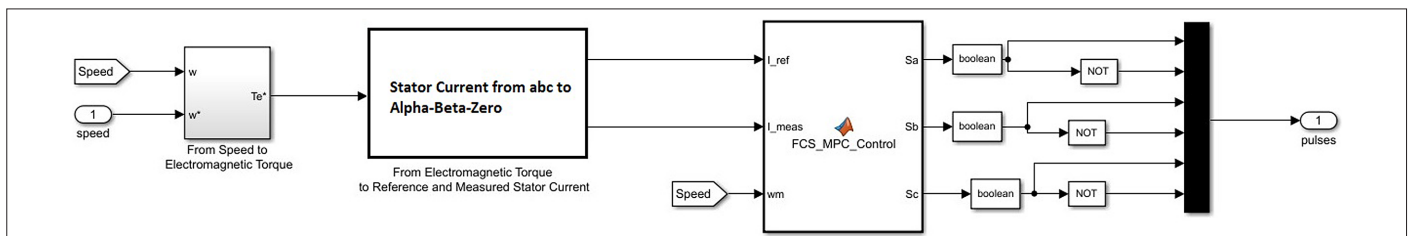
the difference in reference speed has undergone a transformation, first to electromagnetic torque and then from electromagnetic torque to alpha-beta-zero stator current. As a result, in Fig. 2, the FCS-MPC model utilizing the difference between reference, measured speed, and stator currents was employed for simulation. The simulation was conducted using MATLAB-Simulink [41].

A. Mathematical Model of Induction Motor

In motors, the mathematical model consists of equations of the electrical and mechanical system. In this model showing the behavior of the motor, the equations expressing the mechanical side are derived from Newton's laws of motion, and the equations expressing the electrical side are obtained from Kirchoff's current laws [42].

The model of the motor according to the stationary $\alpha\text{-}\beta$ axes rotating with any angular speed $4 \omega_m$ is as in (1) [42].

$$\begin{bmatrix} \frac{di_{s\alpha}}{dt} \\ \frac{di_{s\beta}}{dt} \\ \frac{d\psi_{r\alpha}}{dt} \\ \frac{d\psi_{r\beta}}{dt} \end{bmatrix} = \begin{bmatrix} -\frac{R_E}{\sigma L_s} & 0 & \frac{L_m R_r}{\sigma L_s L_r^2} & p\omega_m \frac{L_m}{\sigma L_s L_r} \\ 0 & -\frac{R_E}{\sigma L_s} & -p\omega_m \frac{L_m}{\sigma L_s L_r} & \frac{L_m R_r}{\sigma L_s L_r^2} \\ \frac{L_m R_r}{L_r} & 0 & -\frac{R_r}{L_r} & -p\omega_m \\ 0 & \frac{L_m R_r}{L_r} & p\omega_m & -\frac{R_r}{L_r} \end{bmatrix} \begin{bmatrix} i_{s\alpha} \\ i_{s\beta} \\ \psi_{r\alpha} \\ \psi_{r\beta} \end{bmatrix} + \begin{bmatrix} \frac{1}{\sigma L_s} & 0 \\ 0 & \frac{1}{\sigma L_s} \\ 0 & 0 \\ 0 & 0 \end{bmatrix} \begin{bmatrix} v_{s\alpha} \\ v_{s\beta} \end{bmatrix} \quad (1)$$



where $\psi_{r\alpha}$, $\psi_{r\beta}$, $i_{s\alpha}$, $i_{s\beta}$, $v_{s\alpha}$ and $v_{s\beta}$ are the rotor flux value in the α -axis, the rotor flux value in the β -axis, the α -axis stator current, the β -axis stator current, the α -axis stator voltage, and the β -axis stator voltage, respectively. The equivalent resistance shown in (2) is utilized in the electrical modeling of the motor and is a parameter employed to represent the behavior of the actual motor.

$$R_E = R_s + \frac{R_r L_m^2}{L_r^2} \quad (2)$$

where R_E , R_s , R_r , L_m , and L_r are the equivalent resistance, the sum of the stator resistance, the rotor resistance, mutual inductance, and rotor inductance, respectively.

The leakage factor, defined in (3) as the ratio of the rotor inductance to the stator, represents the incurred inductance loss in the motor.

$$\sigma = 1 - \frac{L_m^2}{L_s L_r} \quad (3)$$

Leakage factor σ affects the operating characteristics of an induction motor and involves the calculation of stator inductance L_s .

The induction motor simulated in our study is of the rotor type squirrel-cage. A squirrel-cage induction machine can be described by a set of equations as given below using the stator current as the reference axis and the induction motor state equations. To simplify the control processes depicted in (4), (5), (6), and (7), the three-phase induction motor is decomposed into α - and β -axis components.

$$\frac{di_s}{dt} = \frac{di_{s\alpha}}{dt} + j \frac{di_{s\beta}}{dt} \quad (4)$$

$$i_s = i_{s\alpha} + j i_{s\beta} \quad (5)$$

$$\psi_r = \psi_{r\alpha} + j \psi_{r\beta} \quad (6)$$

$$v_s = v_{s\alpha} + j v_{s\beta} \quad (7)$$

where i_s , ψ_r , and v_s are the stator current, the rotor flux value, and stator voltage value, respectively.

$$\frac{di_s}{dt} = -\frac{R_E}{\sigma L_s} i_s + \left(\frac{L_m R_r}{\sigma L_s L_r^2} - j p \omega_m \frac{L_m}{\sigma L_s L_r} \right) \psi_r + \frac{1}{\sigma L_s} v_s \quad (8)$$

$$\frac{d\psi_r}{dt} = \frac{L_m R_r}{L_r} i_s + \left(j p \omega_m - \frac{R_r}{L_r} \right) \psi_r \quad (9)$$

Equation (10) represents the voltage equation of the phase winding.

$$v_s = i_s R_s + \frac{d}{dt} \psi_s \quad (10)$$

Since a squirrel cage induction motor is considered in (11), the rotor voltage vector is equal to zero. Therefore, the rotor winding is short-circuited.

$$i_r R_r + \frac{d}{dt} \psi_r - j p \omega_m \psi_r = 0 \quad (11)$$

Stator flux ψ_s and rotor flux ψ_r are calculated using (12) and (13). The electromagnetic torque T_e is proportional to the imaginary component of the product of the stator flux equivalent and the stator current, as seen in (14). Considering the mechanical equation of the rotor, it can be seen that the torque is related to the mechanical rotor speed ω_m .

$$\psi_s = L_s i_s + L_m i_r \quad (12)$$

$$\psi_r = L_r i_r + L_m i_s \quad (13)$$

$$T_e = \frac{3}{2} p \text{Im} \{ \psi_s^* i_s \} = -\frac{3}{2} p \text{Im} \{ \psi_r^* i_r \} \quad (14)$$

The rotational inertia of the motor and its resistance to changes in speed is described in (15).

$$J \frac{d}{dt} \omega_m = T_e - T_l \quad (15)$$

where J , T_l , ω_m , and ω_r are the moment of inertia of the motor, the load torque, rotor angular velocity, and rotor currents angular velocity, respectively.

The relationship between the stator currents and mechanical rotor angular velocity according to the number of pole pairs is shown in (16).

$$\omega_s = \omega_r + p \omega_m \quad (16)$$

B. Model Predictive Control Method

Model predictive control has evolved significantly over the past two decades. This success can be attributed to the fact that MPC is perhaps the most general way to pose the process control problem in the time domain. As mentioned in Fig. 3 in the MPC method, the output of the system is used directly to obtain the feedback input [43].

In Fig. 3, the fundamental representation of the optimized future inputs, derived based on past inputs and outputs for tracking the reference signal using MPC, is depicted.

In MPC, the cost function that facilitates the optimization of the generated signal for tracking a reference signal is represented in terms of outputs and inputs, as shown in (17).

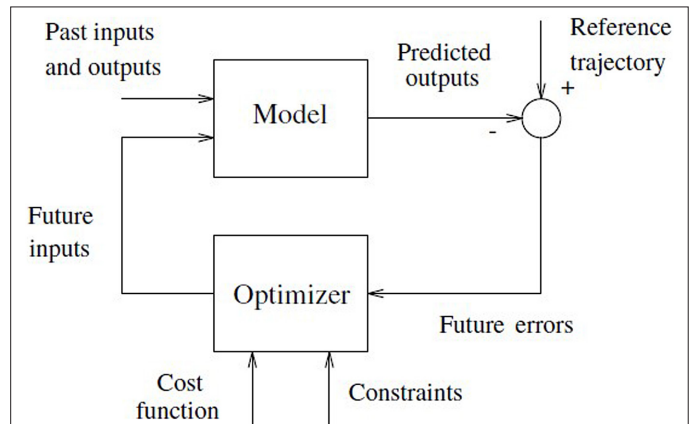


Fig. 3. Basic structure of MPC [43].

$$J = \sum_{j=1}^p \delta \left[\check{y}(t+j|t) - w(t+j) \right]^2 + \sum_{j=1}^m \lambda \left[\Delta u(t+j-1) \right]^2 \quad (17)$$

where J is the cost function; p is the prediction horizon; m is the control horizon; δ is the coefficient of difference between reference output and produced output; λ is the coefficient of manipulated input; j is the next step according to discrete time; $\check{y}(t+j|t)$ is the output produced by MPC; $w(t+j)$ is the referenced output; and Δu is the manipulated control input increment [43].

C. Cost Function Discretization Methods

In practical application of control systems for IM, the controller discretizes the feedback signals received from the motor. Control algorithms are then used based on these discretized signals. By modifying the discretization methods used in the control algorithm, the motor's responses and measured outcomes can be altered. In this study, the currents utilized in the cost function of model predictive current control (MPCC) implemented in a finite control set are discretized using different methods.

When investigating the discretization methods used in MPC in the literature, it has been observed that a significant portion of the studies is conducted using the Forward Euler method. The Forward Euler method works well when the function is linear or close to linear; however, it may lead to significant errors otherwise. To solve this problem, the sampling time, or step size, is reduced. In the Forward Euler formula in (18), the value of x_k in the next step is calculated by multiplying the first derivative of x_k by the sampling time T_s and adding it to x_k .

$$x_{k+1} \approx x_k + T_s \left. \frac{d}{dt} x \right|_{x_k} \quad (18)$$

where x_k is the system state variable and x_{k+1} is the next state variable.

The Taylor series method is given in (19). The first-order Taylor series expansion is identical to the Forward Euler method.

$$x_{k+1} \approx x_k + T_s \left. \frac{d}{dt} x \right|_{x_k} + \frac{T_s^2}{2} \left. \frac{d^2}{dt^2} x \right|_{x_k} + \frac{T_s^3}{3!} \left. \frac{d^3}{dt^3} x \right|_{x_k} + \dots \quad (19)$$

The Runge–Kutta fourth order method is given in (21). The step size for the derivative is formed by the combination of four different coefficients.

$$\begin{aligned} r_1 &= f(x_k, u_k) \\ r_2 &= f\left(x_k + \frac{T_s}{2} r_1, u\left(t_k + \frac{T_s}{2}\right)\right) \\ r_3 &= f\left(x_k + \frac{T_s}{2} r_2, u\left(t_k + \frac{T_s}{2}\right)\right) \\ r_4 &= f(x_k + T_s r_3, u(t_k + T_s)) \end{aligned} \quad (20)$$

$$x_{k+1} = x_k + \frac{T_s}{6} (r_1 + 2r_2 + 2r_3 + r_4) \quad (21)$$

where Runge–Kutta fourth order coefficients are r_1 , r_2 , r_3 , and r_4 . System control input is u_k .

The Runge–Kutta Ralston method is derived from the Runge–Kutta 4 method. As shown in (23), the Ralston method employs fewer steps compared to Runge–Kutta 4.

$$\begin{aligned} r_1 &= f(x_k, u_k) \\ r_2 &= f\left(x_k + \frac{3}{4} T_s r_1, u_k + \frac{3}{4} T_s r_1\right) \end{aligned} \quad (22)$$

$$x_{k+1} = x_k + \left(\frac{1}{3} r_1 + \frac{2}{3} r_2\right) T_s \quad (23)$$

where Runge–Kutta Ralston order coefficients are r_1 and r_2 .

The Crank–Nicolson method is an implicit method, and its differentiation from the Runge–Kutta methods is in its capability, as demonstrated in (25), to amalgamate forward and backward time steps.

$$\frac{dx}{dt} = f(x, t) \quad (24)$$

$$\frac{x^{k+1} - x^k}{T_s} = \frac{1}{2} \left[f(x^k, t^k) + f(x^{k+1}, t^{k+1}) \right] \quad (25)$$

Verlet integration method, in contrast to the Crank–Nicolson method, utilizes the value one step behind, as demonstrated in (28), in solving differential equations.

$$\frac{dx}{dt} = f(x, t) \quad (26)$$

$$x_{\text{prev}} = x(\text{previous time step}) \quad (27)$$

$$x = 2x - x_{\text{prev}} + T_s^2 \cdot f(x, t) \quad (28)$$

where x is a variable belonging to the function $f(x, t)$ and x_{prev} is the variable of x from the previous step.

D. IFOC Method

The reference current components and transformation angle of the induction motor obtained through the IFOC method are converted to three-phase stator currents. The transformed reference currents are compared with the data from current sensors and brought within the hysteresis band, resulting in pulse width modulation (PWM) signals. The acquired PWM signals serve as gate signals for the inverter and supply it with power [43].

E. The Total Harmonic Distortion

In induction motors, power transmission systems such as motor speed and direct current link voltage are prone to fluctuations. Due to its expandable nature, the FCS-MPC method can be employed to minimize torque and flux fluctuations, which are among the causes of harmonic oscillations [43, 44]. The nonlinear loads powered from the voltage source generate a distorted waveform with harmonics. These harmonics can lead to various issues in induction motors, including conductor and insulation material degradation. Consequently, it is important to determine the full extent of the impact of these harmonics. The THD of a system refers to the sum of all harmonics present in the system. Harmonic distortion is a term commonly used to describe the amount of harmonic content present in an alternating signal [45].

III. COMPARISON OF APPLIED DISCRETIZATION METHODS

In this study, a finite control set MPCC method is proposed to ensure the reference speed tracking of the induction motor. The reason for using FCS-MPC is its practicality and the ease with which coefficients of the cost function can be developed based on human observation [46]. With the proposed control method, induction motor speed transitions are adjusted according to the system to be used, thereby reducing the overshoot and settling time values.

In this study, the working principles, advantages, and application areas of FCS-MPC for induction motors have been examined. The FCS-MPC method emerges as an effective solution for speed and current control in the utilized induction motors. Finite control set model predictive control is an advanced control strategy employed to predict system behavior and compute control signals using a mathematical model. This control strategy solves an optimization problem to determine the most appropriate control signals for the subsequent step within a specific control period. The resolution of this optimization problem is based on the optimization of cost functions. In this optimization process, the accurate discretization and control of stator currents play a significant role. This study examines the advantages provided by different discretization methods of stator currents in the cost function. The selection of appropriate discretization methods according to the requirements significantly impacts the motor's control strategy and performance. Therefore, an algorithm flowchart has been developed for FCS-MPC, depicted in Fig. 4. The innovation in the rules shown in Fig. 4 for the induction motor involves the utilization of various mathematical discretization methods, namely Forward Euler, Taylor series, Verlet integration, Crank–Nicolson, Runge–Kutta 4, and Runge–Kutta Ralston, in the calculation of stator current. Thus, in the proposed different control methods, the error between the reference speed and the measured speed of the induction motor is maintained at a minimum value. In Fig. 4, V_{dc} , T_s , J , L_m , L_r , L_s , R_r , R_s , I_{ref} , I_{meas} , ω_m , and I_{k1} are voltage, sampling time, motor inertia value, mutual inductance value, rotor inductance value, stator inductance value, rotor resistance value, stator resistance value, reference current, measured current, angular velocity, and predicted current value, respectively. With these values given in Fig. 4, the stator current I_{k1} that we defined in MATLAB–Simulink is calculated, and then the calculated stator current I_{k1} is converted into a cost function with reference values. The value obtained from the cost function (g) is compared with the previously determined cost function (g_{opt}) scalar value. The transition continues as long as the cost function value is less than the predetermined optimal cost function value.

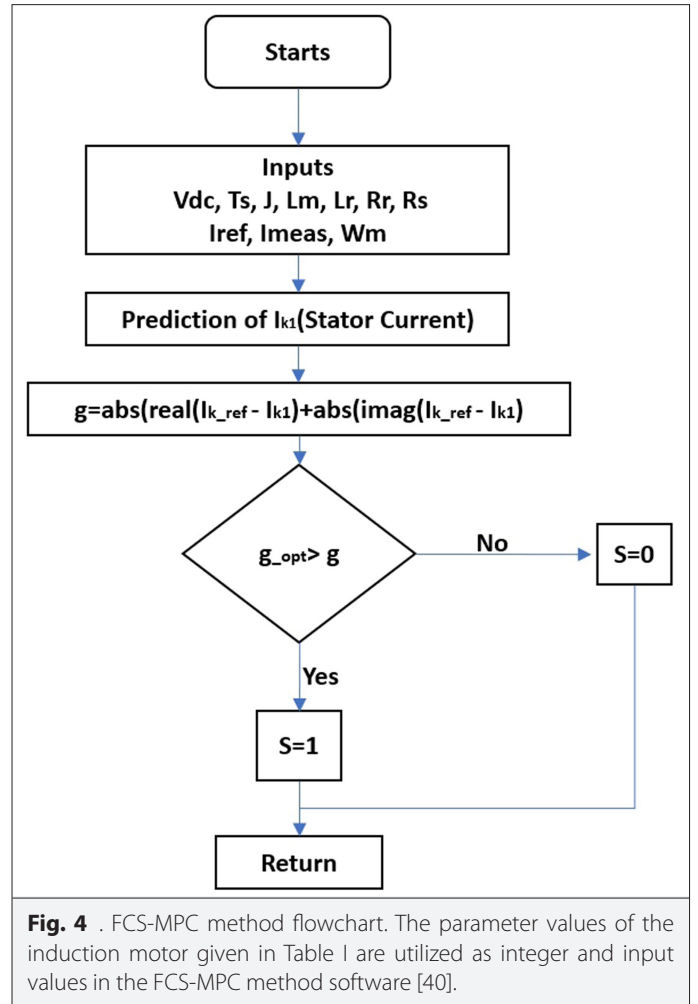
When Table I and Fig. 4 are examined, two fundamental input parameters determining the operation of the induction motor at desired speeds are identified. These are the predicted stator current and the cost function values.

The Forward Euler discretization method [46], given by the following equations, was chosen as the primary discretization method.

$$k_r = \frac{L_m}{L_r} \quad (29)$$

$$r_\sigma = R_s + k_r^2 R_r \quad (30)$$

$$t_\sigma = \frac{\sigma L_s}{r_\sigma} \quad (31)$$



$$F_r = \frac{L_r}{L_m} F_s + i_k \left(L_m - \frac{L_r L_s}{L_m} \right) \quad (32)$$

$$i_{k1} = \frac{t_\sigma}{t_\sigma + T_s} i_k + \frac{T_s}{t_\sigma + T_s} \left(\frac{1}{r_\sigma} \left(\frac{k_r}{t_r} - k_r j \omega_m \right) F_r + v_{o1} \right) \quad (33)$$

where k_r , r_σ , t_σ , F_r , and F_s are the coefficient of mutual inductance, the rotor's electrical resistance, the time constant of losses, the magnetic force of the motor, and the stator current-related magnetic force, respectively.

The Forward Euler method directly computes the estimated rate of change, which is the derivative of the variable at the next time step. This method is preferred due to its simple structure and ease of implementation, forming the basis of discretization methods, and is typically used first in systems where control will be applied. The Runge–Kutta 4 method calculates split sampling time values to calculate the next step more accurately. While this method involves more complex mathematical calculations and heavier computational load, it provides more precise results. The Crank–Nicolson method calculates the next step by taking the average of past and future steps, whereas the Forward Euler method directly computes the next step. The Crank–Nicolson method tends to produce more accurate results because it uses information from both current and future steps. The Runge–Kutta Ralston method uses two estimates to

TABLE I. INDUCTION MOTOR PARAMETERS [40]

Parameters	Value
Stator resistance	0.087 Ω
Rotor resistance	0.228 Ω
Stator and rotor inductance	0.8e-3H
Mutual inductance	34.7e-3H
Inertia	1.662 kg/m ²
Pole pair	2
Friction factor	0.1 Nm/s
Nominal power	50 HP
Rated speed	1780 Nm
Voltage	460 V
Frequency	60 Hz

calculate the next step based on the previous step. It offers a more balanced approach, generally performing better in a variety of electromechanical systems with nominal high speeds. The Taylor series method is expressed as an expanded approximate series of a function, providing higher accuracy by including higher-order derivatives. Verlet integration calculates the next step using the current position and velocity. It uses second-order differential equations and predicts the next position and velocity using the current ones. Verlet integration is generally more balanced in terms of system dynamics due to features such as conservation of energy and Hamiltonian mechanics.

TABLE II. IFOC PI PARAMETERS [40]

The values	Coefficients
Proportional (Kp)	13
Integral (Ki)	26
Torque limit (N/m)	300

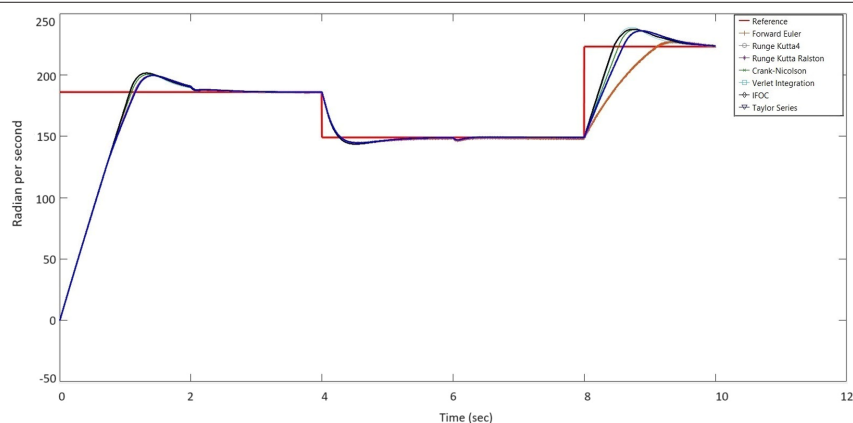
Additionally, the values of the proportional and integral controllers used in the classical control method, IFOC, for speed-to-electromagnetic torque conversion are provided in Table II [41]. Unlike MPC methods, IFOC does not use as much mathematics in calculations as MPC.

IV. SIMULATION RESULTS AND DISCUSSION

In this simulation study, FCS-MPC discretization methods including Forward Euler, Runge–Kutta 4, Runge–Kutta Ralston, Crank–Nicolson, Verlet integration, Taylor series, and the conventional IFOC method were examined. The output signals for the speed tracking control of the induction motor using FCS-MPC methods and the IFOC method are shown in Fig. 5.

The zoomed signals for the speed tracking control of this induction motor are for 0–4 s in Fig. 6a, for 8–10 s in Fig. 6b, and for 4–6 s in Fig. 7. The arrows indicate the settling times and overshoot percentage values in all figures. When the induction motor operates without load, with the nominal operating speed selected as the reference speed, the percentage overshoot and settling time values are shown in Fig. 6a. A detailed representation of the speed variation between 8 and 10 s of Fig. 5 is provided in Fig. 6b. This includes the transition from 149 rad/s (20% decrease from the nominal speed) to 223 rad/s (20% increase from the nominal speed).

When between 0 and 4 s positive region (at 186 rad/s speed) in Fig. 6a are examined, it is seen that Verlet integration method has the least settling time value as 1.624 s, while Taylor series, Runge–Kutta 4, and Runge–Kutta Ralston methods have the least overshoot percentage value as 7.26. When between 4 and 8 s negative region (at 149 rad/s speed) are examined in Fig. 7, it is seen that Verlet integration method has both the least settling time value and overshoot percentage value. When between 8 and 10 s positive region (at 223 rad/s speed) are examined in Fig. 6b, it is seen that the Forward Euler method has both the least settling time value and overshoot percentage value. When examining Fig. 7, it is observed that the motor speed decreases from the nominal speed of 186–149 rad/s. In Fig. 7, when comparing the negative region overshoot values, it has been observed that all discretization methods belonging to FCS-MPC exhibit less overshoot percentage compared to the IFOC method.

**Fig. 5.** The output signals for speed tracking of an induction motor.

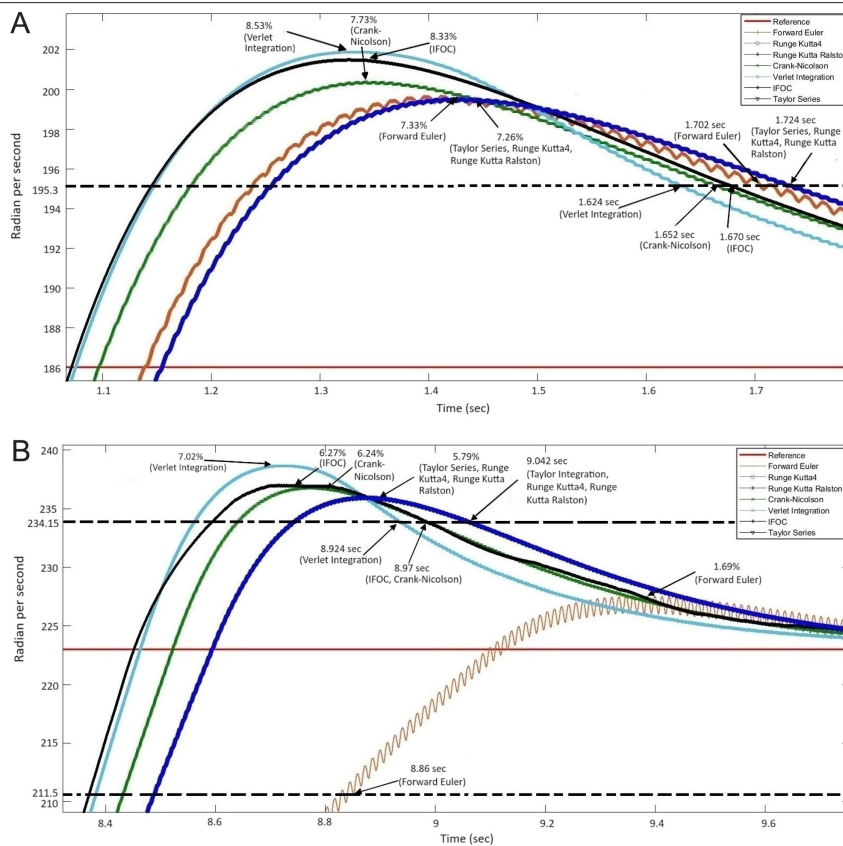


Fig. 6. (a) Transient responses in positive region (186 rad/s speed). (b) Transient responses in positive region (223 rad/s speed).

Fig. 8 shows the effect of electromechanical torque on the reference speed.

In Fig. 9, a mechanical torque of 100 Nm is applied to the induction motor in the form of a pulse at the “second” second within the +5% error band of the 186 rad/s reference speed, as shown in Fig. 8. It is observed that the applied torque does not cause the motor to deviate outside the error band of the reference speed. Considering the speed peak value as a result of the electromechanical torque applied to the reference speed, Taylor series, Runge–Kutta 4, and

Runge–Kutta Ralston discretization methods have higher speed peak values than all other methods.

In Fig. 10, during the tracking of the reference speed of 149 rad/s with a near-zero error band, a mechanical torque of 100 Nm was applied to the induction motor at sixth seconds. Similar to Fig. 9, the applied mechanical torque did not cause the motor to deviate outside the band of the reference speed. In the results obtained in Fig. 10, IFOC and Crank–Nicholson discretization methods have similar peak values with other methods except the Forward Euler discretization

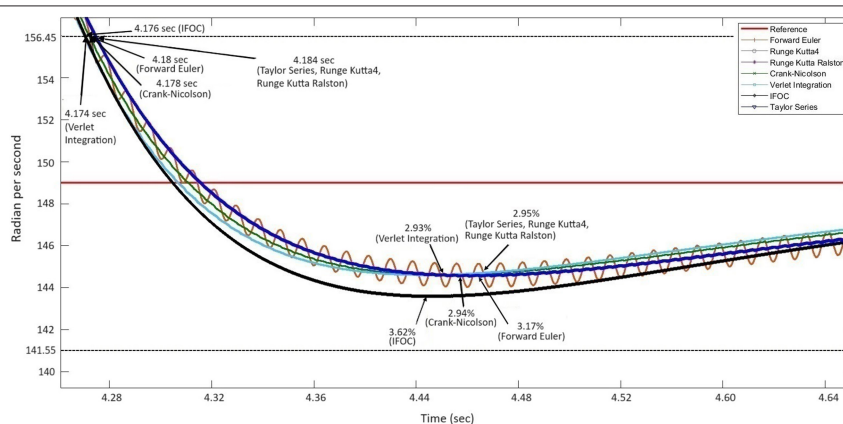


Fig. 7. Transient responses in negative region (149 rad/s speed).

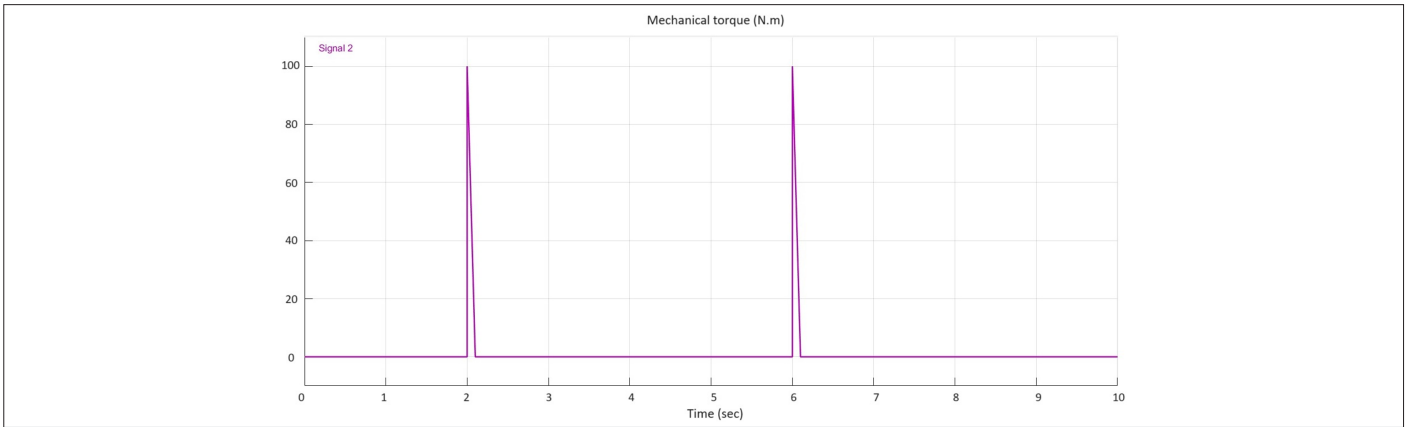


Fig. 8. The applied electromechanical torque value.

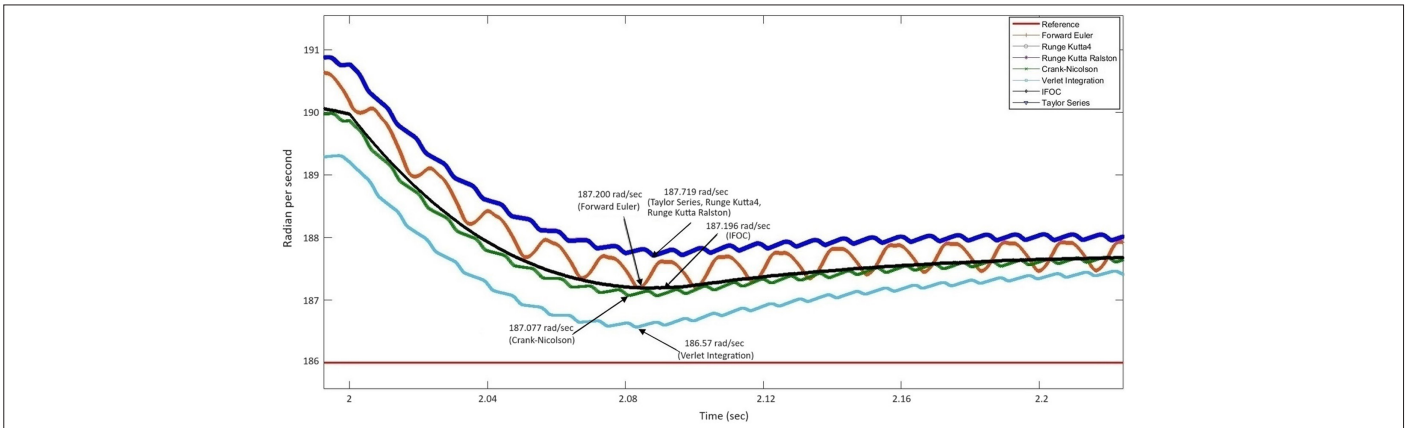


Fig. 9. The responses to the applied mechanical torque at "second" seconds.

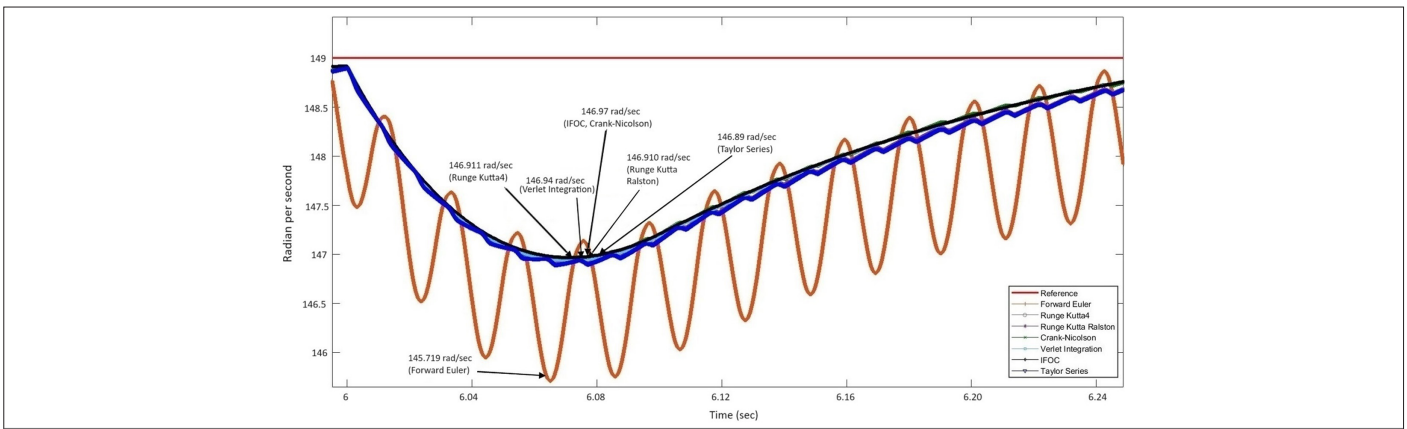


Fig. 10. The responses to the applied mechanical torque at sixth seconds.

method. It was observed that the Forward Euler method exhibits more switching noise in response to applied torque at speeds lower than the nominal speed of the induction motor compared to all other methods.

Table III shows peak values of the responses to the applied mechanical torque at second seconds and sixth seconds for FCS-MPC discretization methods and IFOC method.

In Fig. 11, overshoot and settling time values were presented in detail in the form of radar charts. In Fig. 11a, the overshoot percentage value of the induction motor at the nominal operating speed (186 rad/s) was largest for the Verlet integration method. This is due to the utilization of position and velocity values in the calculation of the next step in the Verlet integration method. The reason why the Taylor series, Runge-Kutta 4, and Runge-Kutta Ralston methods yield similar results and have less overshoot compared to other methods is

TABLE III. RESPONSES TO APPLIED ELECTROMECHANICAL TORQUE

FCS-MPC Discretization Methods and IFOC Method	Electromechanical Torque Applied in 2nd Seconds	Electromechanical Torque Applied in 6th Seconds
	Peak Value of the Negative Region (Speed Response rad/s)	Peak Value of the Negative Region (Speed Response rad/s)
Forward Euler	187.200	145.719
Runge–Kutta 4	187.719	146.911
Runge–Kutta Ralston	187.719	146.910
Crank–Nicolson	187.077	146.97
Verlet integration	186.57	146.94
IFOC	187.196	146.97
Taylor series	187.719	146.890

attributed to the second-order differential equation nature of the cost function. These three methods are achieved by refining the step interval used in Euler methods.

The transient regime parameter values corresponding to a 20% increase in the nominal speed of the induction motor are provided in Fig. 11b and d. Here, the speed of the induction motor operating at 149 rad/s for 4 s is increased to 223 rad/s. Since the step interval used in the Forward Euler method is constant, it is expected to exhibit faster response in simple systems according to the calculation method. However, due to the utilization of a high-power induction motor, the inertia of the motor itself needs to be taken into account. When Fig. 11b and d are examined, it is seen that the Forward Euler has the smallest overshoot percentage and settling time compared to other methods. In Fig. 11c, the settling time value

of the induction motor at nominal speed (186 rad/s) is examined for all methods. Among the methods using Verlet integration, it has the smallest settling time value.

The RMS values of the speeds obtained by IFOC and FCS-MPC methods for the induction motor simulated for 10 s in this study are presented in Table IV. Upon examining Table IV with respect to the reference speed RMS (rad/s) values, it is determined that the Taylor series method is the closest to the reference speed in terms of speed tracking.

Table V shows the percentage overshoot values and settling times of all methods used in controlling the simulated induction motor at speeds of 186 rad/s (positive region), 149 rad/s (negative region), and 223 rad/s (positive region). When between 0 and 4 s positive

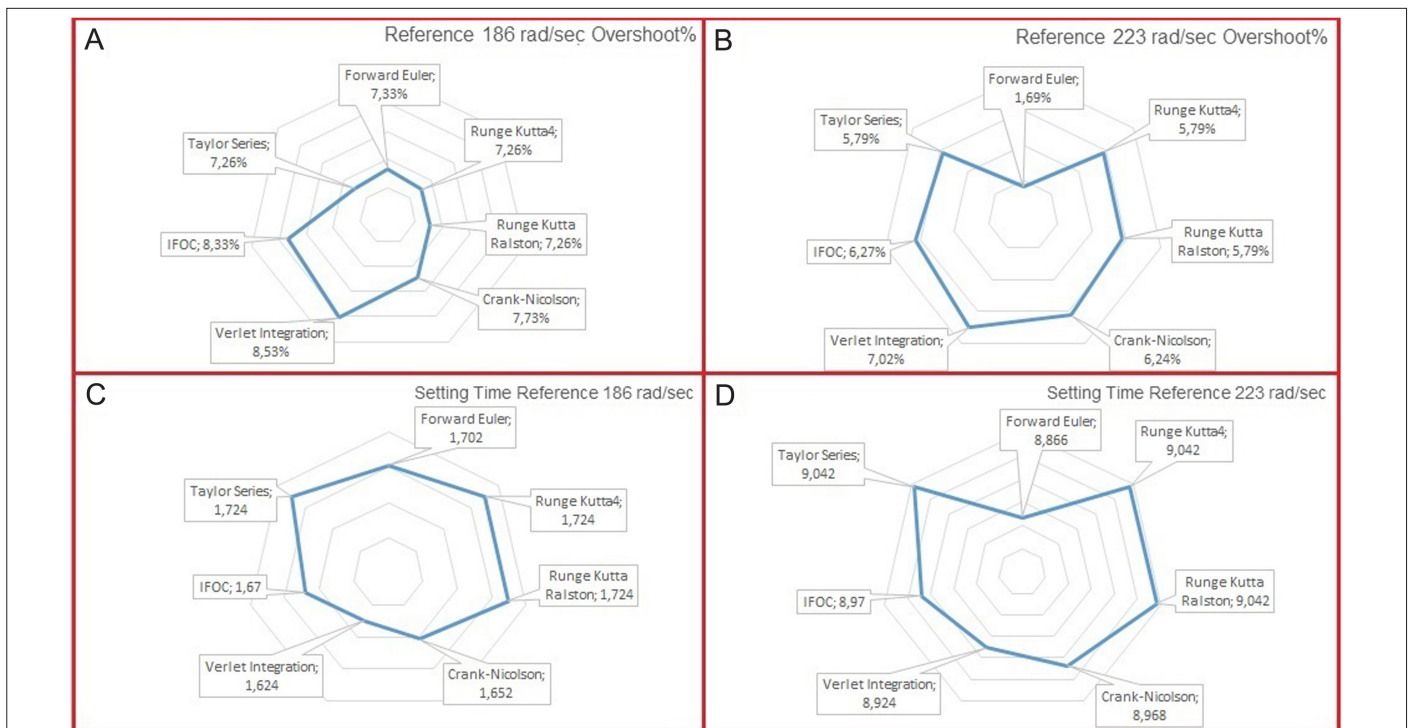


Fig. 11. (a) Radar charts for overshoot percentages comparison at 186 rad/s. (b) Radar charts for overshoot percentage comparison at 223 rad/s. (c) Radar charts for settling time comparisons at 186 rad/s. (d) Radar charts for overshoot percentages comparison at 223 rad/s.

TABLE IV. THE SPEED RMS VALUES OF THE SIMULATED INDUCTION MOTOR SPEED

The Utilized Control Methods	Speed RMS (rad/s)
Reference	180.7
FCS-MPC Forward Euler	170.8
FCS-MPC Verlet integration	174.3
FCS-MPC Crank–Nicolson	170
FCS-MPC Taylor series	174.5
FCS-MPC Runge–Kutta Ralston	173.5
FCS-MPC Runge–Kutta 4	173.5
IFOC	174.3

region (at 186 rad/s speed) are examined, it is seen that Verlet integration method has the least settling time value as 1.624 s while Taylor series, Runge–Kutta 4, and Runge–Kutta Ralston methods have the least overshoot percentage value as 7.26. When between 4 and 8 s negative region (at 149 rad/s speed) are examined, it is seen that Verlet integration method has both the least settling time value and overshoot percentage value. When between 8 and 10 s positive region (at 223 rad/s speed) are examined, it is seen that the Forward Euler method has both the least settling time value and overshoot percentage value.

On the other hand, harmonic distortion percentage values occurring during the control of the induction motor are presented in Table VI. It has been observed that the FCS-MPC methods produce more harmonics than the classical IFOC method due to the large number of switching signals and mathematical operations. This phenomenon can be attributed to the dynamic nature of the switching signals produced by FCS-MPC methods, as opposed to the linear structure used in the IFOC method.

V. CONCLUSION

In this paper, we compared the Forward Euler, Runge–Kutta 4, Runge–Kutta Ralston, Taylor Series, Crank–Nicolson, and Verlet Integration techniques, which are FCS-MPC methods, with the

TABLE VI. STATOR CURRENT HARMONIC DISTORTION VALUES

IM Control Type	Stator Current Harmonic Distortion (%)			
	0–4 s	4–6 s	6–8 s	Three Different Seconds Average
IFOC	8.28	30.33	38.36	25.66
FCS-MPC Forward Euler	21.73	55.21	41.58	39.51
FCS-MPC Verlet integration	33.35	43.67	25.84	34.29
FCS-MPC Crank–Nicolson	12.67	48.59	28.33	29.86
FCS-MPC Taylor series	25.59	56.83	32.63	38.35
FCS-MPC Runge–Kutta Ralston	25.48	56.8	31.85	38.04
FCS-MPC Runge–Kutta 4	25.59	56.83	32.48	38.30

conventional IFOC method for speed control of induction motors. The results indicated that the Taylor series discretization method exhibited an RMS value close to the reference speed compared to other methods for induction motor speed control. It was seen that the method furthest from the reference speed RMS value was the Crank–Nicolson method. This was attributed to the averaging of past and future steps in calculating the next step.

When analyzing the reference speed tracking of both unloaded and loaded conditions, the Taylor series method exhibited similar results to the Runge–Kutta 4 and Runge–Kutta Ralston methods. When the mechanical load response of the induction motor after reaching its nominal speed from zero speed was examined, it was seen that Taylor, Runge–Kutta 4, and Runge–Kutta Ralston methods gave smaller overshoot percentage values than other methods. When response signals were examined between 0 and 4 s at 186 rad/s speed, it was seen that Verlet integration method had the least settling time value as 1.624 s, while Taylor series, Runge–Kutta 4, and Runge–Kutta Ralston methods had the least overshoot percentage value as 7.26. When comparing the overshoot percentage values for between 4 and 10 s, the reason for the higher overshoot value of the IFOC method compared to other methods was the linear controller coefficients minimizing the current error at constant values. When response signals were examined between 4 and 8 s at 149 rad/s speed, it was seen that Verlet integration method has both the least

TABLE V. TRANSIENT REGIME CRITERIA FOUND FROM SIMULATIONS FOR THE INDUCTION MOTOR

FCS-MPC Discretization Methods and IFOC Method	Positive Region (Between 0 and 4 s) at 186 rad/s Reference Speed		Negative Region (Between 4 and 8 s) at 149 rad/s Reference Speed		Positive Region (Between 8 and 10 s) at 223 rad/s Reference Speed	
	Settling Time (s)	Overshoot (%)	Settling Time (s)	Overshoot (%)	Settling Time (s)	Overshoot (%)
Forward Euler	1.702	7.33	4.18	3.17	8.86	1.69
Runge–Kutta 4	1.724	7.26	4.184	2.95	9.042	5.79
Runge–Kutta Ralston	1.724	7.26	4.184	2.95	9.042	5.79
Crank–Nicolson	1.652	7.73	4.178	2.94	8.97	6.24
Verlet Integration	1.624	8.53	4.174	2.93	8.924	7.02
IFOC	1.670	8.33	4.176	3.62	8.97	6.27
Taylor Series	1.724	7.26	4.184	2.95	9.042	5.79

settling time value and overshoot percentage value. When response signals were examined between 8 and 10 s at 223 rad/s speed, it was seen that Forward Euler method had both the least settling time value and overshoot percentage value. Furthermore, when investigating the response to the mechanical load given at 80% of the nominal speed of the induction motor, it was observed that, except for the Forward Euler method, the other methods yielded similar results of minimal switching loss.

When examining the current harmonic values generated by the induction motor driven using FCS-MPC control methods, it was observed that the Crank–Nicolson discretization method exhibited less harmonic distortion compared to other FCS-MPC methods. The reason for this is the Crank–Nicolson discretization method's utilization of both the future and current steps in predicting the next step calculation. It is a well-known fact in the literature that the IFOC method generally produces fewer harmonics compared to MPC due to the reduced switching operations. In future work, we plan to experimentally verify these theoretical findings on an induction motor in real time.

Peer-review: Externally peer-reviewed.

Author Contributions: Concept –Y.K., N.B.; Design –Y.K., N.B.; Supervision –N.B.; Resources –Y.K.; Materials –N.B.; Data Collection and/or Processing –Y.K., N.B.; Analysis and/or Interpretation –N.B.; Literature Search –Y.K.; Writing –Y.K., N.B.; Critical Review –N.B.

Declaration of Interests: The authors have no conflict of interest to declare.

Funding: The authors declared that this study has received no financial support.

REFERENCES

- D. W. Novotny, and T. A., "Monographs in electrical and electronic engineering", in *Lipo, Vector Control and Dynamics of AC Drives*. Oxford: Clarendon Press, 1996.
- S. Lee, and K. Lee, "Current measurement offset error compensation for IFOC induction motor drives," *IEEE Trans. Ind. Appl.*, vol. 59, no. 4, pp. 4130–4139, 2023. [\[CrossRef\]](#)
- S. K. Kakodia, and G. Dynamina, "A comparative study of DFOC and IFOC for IM drive," in *Control Autom. (ICMICA), Kurukshetra, India*. First IEEE International Conference on Measurement, Instrumentation. [\[CrossRef\]](#)
- B. K. Bose, "Modern power electronics and AC Drives" *PHI Learning*, 2002.
- R. J. Wai, and K. M. Lin, "Robust decoupled control of direct fieldoriented induction motor drive," *IEEE Trans. Ind. Electron.*, vol. 52, no. 3, pp. 837–854, 2005. [\[CrossRef\]](#)
- D. Giribabu, S. P. Srivastava, and M. K. Pathak, "Rotor flux based MRAS for sensorless operation of three level inverter fed induction motor," in *IEEE Students' Conference on Electrical, Electronics and Computer Science: Innovation for Humanity, SCEECS*, vol. 2012, 2012, pp. 1–4. [\[CrossRef\]](#)
- E. Dehghan-Azad, S. Gadoue, D. Atkinson, H. Slater, P. Barrass, and F. Blaabjerg, "Sensorless control of IM based on stator-voltage MRAS for Limp-Home EV applications," *IEEE Trans. Power Electron.*, vol. 33, no. 3, pp. 1911–1921, 2018. [\[CrossRef\]](#)
- F. AtAllah, S. Mukhopadhyay, H. Rehman, and H. A. Khalid, "Battery temperature assessment for FOPi and PI based electric vehicle traction system," in *International Conference on Fractional Differentiation and Its Applications (ICFDA), Ajman, United Arab Emirates*, 2023, pp. 1–6. [\[CrossRef\]](#)
- M. S. Sepeeh, S. A. Zulkifli, S. S. Yi, and H. -J. Chiu, "Motor speed control based on enhanced indirect-field-oriented control using convolutional neural network," in *IECON 49th Annual Conference of the IEEE Industrial Electronics Society, Singapore*, 2023, pp. 1–6. [\[CrossRef\]](#)
- E. Zerdali, M. Rivera, P. Zanchetta, P. Wheeler, and L. Ristić, "Encoderless predictive speed and torque control of an induction motor," in 22nd International Symposium on Power Electronics (EE), Novi Sad, Serbia, 2023, pp. 1–6. [\[CrossRef\]](#)
- S. Odhano, R. Bojoi, A. Formentini, P. Zanchetta, ve A. Tenconi, "Direct flux and current vector control for induction motor drives using model predictive control theory," *IET Electr. Power Appl.*, vol. 11, no. 8, pp. 1483–1491, 2017. [\[CrossRef\]](#)
- Q. Qian, D. Dongmei, L. Feng, and T. Yongchuan, "Stabilization of the double inverted pendulum based on discrete-time model predictive control," in IEEE International Conference on Automation and Logistics (ICAL), Chongqing, China, 2011, pp. 243–247. [\[CrossRef\]](#)
- T. Liu, X. Yao, J. Wang, and C. Ma, "Efficient Two-Vector-Based Sequential Model Predictive Control for IM Drives," *IEEE J. Emerg. Sel. Topics Power Electron.*, vol. 12, No. 1, 903–912, 2023. [\[CrossRef\]](#)
- I. Hammoud et al., "On continuous-set model predictive control of permanent magnet synchronous machines," *IEEE Trans. Power Electron.*, vol. 37, no. 9, pp. 10360–10371, 2022. [\[CrossRef\]](#)
- X. Liu et al., "XLiu et al., 'Event-Triggered Neural-Predictor-Based FCS-MPC for MMC,'" *IEEE Trans. Ind. Electron.*, vol. 69, no. 6, pp. 6433–6440, 2022. [\[CrossRef\]](#)
- Z. Wang, Z. Zheng, Y. Li, ve J. Sun, "An offset-free robust model predictive control with incremental model and improved current observer for induction motor," *Int. Trans. Electr. Energ. Syst.*, vol. 29, no. 12, 2019. [\[CrossRef\]](#)
- U. Maeder, and M. Morari, "Offset-free reference tracking with model predictive control," *Automatica*, vol. 46, no. 9, pp. 1469–1476, 2010. [\[CrossRef\]](#)
- S. K. Kim, D. K. Choi, K. B. Lee, and Y. I. Lee, "Offset-free model predictive control for the power control of three-phase AC/DC converters," *IEEE Trans. Ind. Electron.*, vol. 62, no. 11, pp. 7114–7126, 2015. [\[CrossRef\]](#)
- A. Abdayem, J. Sawma, F. Khatounian, E. Monmasson, and R. Ghosn, "Single prediction horizon finite control set model predictive control for single-phase MMCs," in 6th International Conference on Renewable Energy for Developing Countries (REDEC), Zouk Mosbeh, Lebanon, vol. 2023, 2023, pp. 100–105. [\[CrossRef\]](#)
- P. Gonçalves, S. Cruz, and A. Mendes, "Finite control set model predictive control of six-phase asymmetrical machines—An overview," *Energies*. MDPI, vol. 12, no. 24, p. 4693, 2019. [\[CrossRef\]](#)
- B. Çavuş, and M. Aktaş, "A new adaptive terminal sliding mode speed control in flux weakening region for DTC controlled induction motor drive," *IEEE Trans. Power Electron.*, vol. 39, no. 1, pp. 449–458, 2024. [\[CrossRef\]](#)
- A. K. Singh, H. Dewangan, S. Venu, and S. Jain, "Model Predictive Control for Nine Phase Induction Motor," *IEEE*, in Third International Conference on Power, Control and Computing Technologies (ICPC2T), Raipur, India, 2024, pp. 657–662. [\[CrossRef\]](#)
- S. Lotfollahzadegan, S. A. Davari, M. S. Mousavi, A. Chegeni, L. Tarisciotti, and J. Rodriguez, "Hexagonal zoning deadbeat model predictive control of induction motor," *IET Electr. Power Appl.*, pp. 1–15, 2024. [\[CrossRef\]](#)
- A. Garcés-Ruiz, S. Riffo, C. González-Castaño, and C. Restrepo, "Model predictive control with stability guarantee for second-order DC/DC converters," *IEEE Trans. Ind. Electron.*, vol. 71, no. 5, pp. 5157–5165, 2024. [\[CrossRef\]](#)
- Y. Cui, W. Huang, N. Su, and F. Bu, "Adaptive full-order observer for induction motor based on bilinear transformation method," in 21st International Conference on Electrical Machines and Systems (ICEMS), 2018, pp. 1649–1653. [\[CrossRef\]](#)
- B. Wang, Y. Zhao, Y. Yu, G. Wang, D. Xu, and Z. Dong, "Speed- sensorless induction machine control in the field-weakening region using discrete speed-adaptive full-order observer," *IEEE Trans. Power Electron.*, vol. 31, no. 8, pp. 5759–5773, 2016. [\[CrossRef\]](#)
- M. Hinkkanen, and J. Luomi, "Novel full-order flux observer structure for speed sensorless induction motors," in IECON. 27th Annual Conference of the IEEE Industrial Electronics Society (Cat. No.37243), vol. 2. USA; 2001, pp. 1333–1338. [\[CrossRef\]](#)
- S. Yin et al., "Improved full-order adaptive observer for sensorless induction motor control in railway traction systems under low- switching frequency," *IEEE J. Emerg. Sel. Top. Power Electron.*, vol. 7, no. 4, pp. 2333–2345, 2019. [\[CrossRef\]](#)
- Y. Zhang, Z. Zhang, O. Babayomi, ve Z. Li, "Weighting factor design techniques for predictive control of power electronics and motor drives," *Symmetry*, vol. 15, no. 6, p. 2023, 1219. [\[CrossRef\]](#)
- O. Gulbudak, M. Gokdag, ve H. Komurcugil, "Model predictive sliding mode control of six-phase induction motor using nine-switch converter," *Int. J. Circ. Theor. Appl.*, vol. 50, no. 10, pp. 3443–3461, 2022. [\[CrossRef\]](#)

31. C. Su, G. Zhang, B. Liu, and Y. Hu, "Model-free predictive control of nonlinear systems based on linearization of partial format," in Chinese Control. and Decision Conference (CCDC), Mianyang, China, 2011, 2011, pp. 2624–2628. [\[CrossRef\]](#)
32. A. Merabet, H. Arioui, and M. Ouhrouche, "Cascaded predictive controller design for speed control and load torque rejection of induction motor," in American Control. Conference, Seattle, WA, USA, 2008, 2008, pp. 1139–1144. [\[CrossRef\]](#)
33. A. Merabet, M. Ouhrouche, and R. -t. Bui, "Nonlinear predictive control with disturbance observer for induction motor drive," in IEEE International Symposium on Industrial Electronics, Montreal, QC, Canada, 2006, pp. 86–91. [\[CrossRef\]](#)
34. C. Garcia, J. Rodriguez, C. Silva, C. Rojas, P. Zanchetta, and H. Abu-Rub, "Full predictive cascaded speed and current control of an induction machine," *IEEE Trans. Energy Convers.*, vol. 31, no. 3, pp. 1059–1067, 2016. [\[CrossRef\]](#)
35. C. A. Rojas, J. I. Yuz, M. Aguirre, and J. Rodriguez, "A comparison of discrete-time models for model predictive control of induction motor drives," in IEEE International Conference on Industrial Technology (ICIT), Seville, Spain, 2015, pp. 568–573. [\[CrossRef\]](#)
36. R. H. Hernández, C. Reusser, M. Coronel, and R. Carvajal, "On accurate discrete-time dynamic models of an induction machine," *Mathematics*, vol. 12, no. 3, p. 373, 2024. [\[CrossRef\]](#)
37. L. Yang et al., "A self-triggered MPC strategy with adaptive prediction horizon for series hybrid electric powertrains," *IEEE Trans. Ind. Inform.*, vol. 20, No. 4, 6762–6771. [\[CrossRef\]](#)
38. N. I. Nahin, S. P. Biswas, M. K. Hosain, M. R. Islam, S. Mondal, ve A. Fekih, *Advanced Model Predictive Control Strategy for Solar PV Fed Induction Motor Drives*, 2023. [\[CrossRef\]](#)
39. B. Çavuş, and M. Aktaş, "Fuzzy logic speed control of induction motor in flux weakening region for electric vehicle," in First International Conference on Cyber Physical Systems, Power Electronics and Electric Vehicles (ICPEEV), Hyderabad, India, 2023, pp. 1–5. [\[CrossRef\]](#)
40. HERE, *Modeling and Simulation of Vector Control System of Alternating Current Motor Based on MATLAB*, 2024.
41. National Defense University, Air Force Academy, Computer Laboratory, Matlab 2019a, Program.
42. G. Bahadır, *Investigation of performances of model predictive controlled induction motors*, M.S.thesis, The Electrical and Electronics Engineering Department at Karabük University Karabük/Turkey, 2018.
43. E. F. Camacho, and C. B. Alba, *Model Predictive Control*. London: Springer, 2013.
44. C. Luo, K. Yang, R. Li, and W. Li, "Predictive compensation-based harmonics suppression for speed-sensorless induction motor drives with improved feedback gains," *IEEE Trans. Transp. Electrifi.*, vol. 10, no. 1, pp. 2135–2144, 2024. [\[CrossRef\]](#)
45. G. Arunkumar, R. Subramanian, U. Arunkumar, and K. S. Chandraguptamauryan, "Estimation of total harmonic distortion in three phase squirrel cage induction motor," in 7th International Conference on Communication and Electronics Systems (ICCES), Coimbatore, India, 2022, pp. 235–240. [\[CrossRef\]](#)
46. L. Wu, and X. Mei, "Predictive current control of an induction machine fed by a two-level voltage source inverter," *IEEE Trans. Ind. Electron.*, vol. 64, no. 4, pp. 2978–2987, 2017.



Yasin Koçak was born in İstanbul. He received his bachelor's degree in electrical engineering from Kocaeli University in 2009. He completed his master's degree in electrical and electronics engineering at İstanbul University in 2014. He is currently pursuing his doctoral studies in the Department of Electronics within the Electrical-Electronics Engineering program at the National Defense University. His research interests include control of electromechanical systems, automatic control systems, control systems design, and model predictive control system modeling.



Nevra Bayhan was born in İstanbul. She received her BSc (Hons.) and MSc degrees in electrical and electronics engineering from İstanbul University in 1997 and 2001, respectively. She completed her PhD in control and automation engineering at İstanbul Technical University in 2008. She is currently an assistant professor at the Electrical and Electronics Engineering Department of İstanbul University-Cerrahpasa. From 2017 to 2022, she worked as the head of Main Scientific Branch Control and Command Systems of Electrical and Electronics Engineering Department, İstanbul University-Cerrahpasa. Her research interests include automatic control systems, control systems design, artificial intelligence, metaheuristic optimization algorithms, time-delay systems, heat transfer in thermoelectric power generation (TEG) and thermoelectric cooling (TEC) systems, system modeling, fuzzy control, low-order controller design, renewable energy systems, robust control, digital control systems, hybrid electric vehicles, and control of systems with parameter uncertainties.